Available online at www.sciencedirect.com
SCIENCE DIRECT®
ELSEVIER
European Journal of Mechanics B/Fluids 22 (2003) 85–97
EUROPEAN JOURNAL OF MECHANICS B/FLUIDS

Flow separation between rotating eccentric cylinders

L.M. de Socio *, L. Marino

Dipartimento di Meccanica e Aeronautica, Universitá "La Sapienza", Via Eudossiana 18, 00184 Roma, Italy

Received 22 May 2002; received in revised form 24 September 2002; accepted 1 October 2002

Abstract

We deal with the dynamic and thermal characteristics of the rarefied flow between two eccentric isothermal cylinders one of which is rotating. A numerical program of direct simulation which is based on a Monte Carlo (DSMC) procedure was adopted and the main results concern the influence of the Knudsen and Mach numbers, and of the eccentricity on the location and extent of the flow separation. Part of the flow domain is shown to be cooler than the wall temperature, and the extent of this region decreases with an increasing gas rarefaction.

1. Introduction

In this paper we consider the flow of a gas between two eccentric cylinders, the outer one of which is rotating. The main purpose of the current work was to evaluate the effects of fluid rarefaction on the characteristics of the thermal field for flow conditions that include separation. The influence of such parameters as the Knudsen and Mach numbers, *Kn* and *Ma*, respectively, at various values of the eccentricity ϵ, will be shown on the location and extent of the separated vortex, in particular, and, more generally, on the fluid flow and thermal fields. In addition the tangential stress and the heat flux will be considered. In this respect the paper represents an investigation on the physical aspects of the problem which is based on a direct simulation Monte Carlo (DSMC) approach. The capabilities and accuracy of the DSMC procedure as it relates to the current problem were discussed in a recent article from a computational point of view [1].

Interest in investigating flow fields which are, at least geometrically, simple lies in the fact that – apart from the possible applications in physics and engineering – they represent standard references and benchmarks, when more complicated situations are dealt with either from the physico-mathematical or the computational point of view. With respect to other analogous important reference situations such as the Couette plane and cylindrical cases and the Poiseuille channel and pipe flows, where one-dimensional problems are dealt with, here a two-dimensional problem is carried out, where a recirculating region can be present even in the very simple Stokes flow.

When one thinks about the extensions and the applications of the results presented here, they span from gas journal bearings to gas centrifuges. A modern book [2] reports a rather exhaustive table of all these applications although it is mostly devoted to the extreme case of gas film lubrication.

The flow between concentric cylinders has been fully studied in the limit situation $\epsilon = 0$, for either a continuum ($Kn \to 0$) medium or for a free molecules gas ($Kn \to \infty$), and the corresponding analytic solutions are available. Numerical and approximate analytic solutions to the compressible slip flow and to the transitional flow at intermediate values of *Kn* are also available [3–5].

For $\epsilon \neq 0$ and $Kn = 0$, $Ma = 0$, the Stokes flow was fully investigated and, in addition, approximate analytic solutions were found to the Navier–Stokes equation by linearization in terms of either ϵ or *Re*, where *Re* is the Reynolds number [6–8]. Also

* Corresponding author.
E-mail addresses: desocio@dma.ing.uniroma1.it (L.M. de Socio), marino@dma.ing.uniroma1.it (L. Marino).

0997-7546/02/$ – see front matter
doi:10.1016/S0997-7546(02)00006-7

Nomenclature

c	sound speed
D	maximum gap between the walls
$\dot{q}$	heat flux
r, α	polar coordinates
u, v	velocity components
x, y	Cartesian coordinates
Kn	Knudsen number
Ma	Mach number
Re	Reynolds number
R	cylinder radius
T	temperature
$\overline{R}$	radii ratio
ξ, η	bipolar coordinates
ϵ	eccentricity
ε	norm
ψ	macroscopic quantity
λ	mean free path
τ	shear stress
ρ	density
Ω	angular speed

Subscripts

0	rest conditions
i	internal wall
e	external wall
cr	critical value

for $\epsilon \neq 0$ and $Kn = 0$, several numerical methods have been applied to obtain solutions for both the incompressible and the compressible flow, $Ma \neq 0$ [9,10]. For large value of Kn, even for the free molecular flow, only numerical results have been presented [11]. In the intermediate Kn regime, to the authors knowledge, no results are present in the literature except those of [1]. Results of Ref. [1] concern a few preliminary calculations of the velocity field to show the convergence and accuracy characteristics of the DSMC procedure used herein.

In the present paper, the focus is on Argon flows at various ϵ, Ma and Kn between two walls at the same temperature. We investigate the influence of Kn on the presence of a separation eddy, the location of its axis, and the angular distance of the separation points on the inner cylinder. Furthermore, the Mach number and temperature fields are presented and discussed as they are affected by changes of the main dimensionless parameters. Also, attention is given to the shear stress and heat flux distributions.

Comparisons are made with reference to the existing data in the limiting case of a continuum medium.

2. Geometry of the problem and direct simulation

As usual in dealing with the geometry of eccentric cylinders, a system of plane bipolar coordinates was considered for solving the motion equations.

The reference frame is therefore represented by two families of orthogonal circles ξ and η as shown in Fig. 1. In such a way ξ_i and ξ_e correspond to the internal and to the external wall of radii R_i and R_e respectively. In the same figure two further

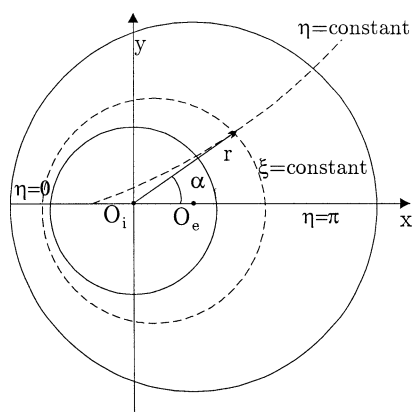

Fig. 1. Geometry of the problem.

reference axes are shown, i.e., a set of Cartesian axes (O_i, x, y) and a set of polar co-ordinates (O_i, r, α) which will be later adopted for particular purposes.

Here $r = R/R_i = (x^2 + y^2)^{1/2}$ and α is measured from x counterclockwise.

We recall that the bipolar coordinates are defined in terms of the dimensionless Cartesian coordinates

$$x = \frac{a \sinh \xi}{\cosh \xi - \cos \eta}, \qquad y = \frac{a \sin \eta}{\cosh \xi - \cos \eta},$$

where the parameter a is given by

$$a = \frac{R_e^2\{1 - (R_i^2/R_e^2)[2 - R_i^2/R_e^2] - (d^2/R_e^2)[2 - d^2/R_e^2 + 2R_i^2/R_e^2]\}^{1/2}}{2R_i \Delta R}$$

with $d = (O_e - O_i)$ the distance between the centers of the two walls and $\Delta R = R_e - R_i$.

Moreover let Ω_e be the angular velocity of the outer cylinder (index e) and c the sound speed of the gas. Let also the index 0 refer to the gas initially at rest between the walls. A set of dimensionless products can be assumed in the form $Ma_e = \Omega_e R_e/c_0$, $Kn_0 = \lambda_0/(R_e - R_i)$, $\overline{R} = R_i/R_e$, $\epsilon = d/\Delta R$, where λ_0 is the mean free path. Then the quantities of main interest are the two velocity components u and v along ξ and η respectively, made non-dimensional with respect to $\Omega_e R_e$, and the density ρ and the temperature T, made dimensionless with respect to their constant values at rest ρ_0^* and T_0^*. The components of the shear stress $\tau \equiv \tau_{\xi\eta}$ and of the heat flux $\dot{q}_\xi$ are dimensionless with respect to $\rho_0^*(\Omega_e R_e)^2$ and $\rho_0^*(\Omega_e R_e)^3$, respectively.

Coming back to the solution procedure, the Monte Carlo simulation was proposed in the past for a number of applications spanning from the dynamics of gases and liquids to the heat transfer in solids. At present, the field where the DSMC methods meet an increasing interest is gasdynamics as a consequence of their relatively simple conceptual foundations and of the development in computational techniques and power. In fact one of the main limitations to a Monte Carlo simulation is its great computer time consumption to obtain a reasonable accuracy in comparison with methods such as finite differences and finite elements when problems in the continuum flow regime are concerned.

The mathematical and physical aspects of the DSMC method have been investigated in a number of papers and textbooks. As a reference we cite here Bird's method, since we developed our computational program from one of the codes reported in [12]. The molecular properties of the gas were also taken from [12] and argon was chosen since its physico-mathematical model best fits the experimental data in a wide range of state conditions. The isothermal walls are assumed perfectly diffusive so that the impinging molecules are re-emitted by sorting their three velocity components from a Maxwellian distribution whose macroscopic parameters, temperature and velocity, are those of the wall.

The accuracy of the numerical procedure has been also discussed in several papers [1,13–15]. We showed in [1] the details concerning the grid characteristics and the number of representative particles as they influence the rate of convergence and the accuracy, after a convergence criterion has been assigned.

In particular we assumed as a criterion that the norm of such parameters as u and ρ

$$\varepsilon_\psi = \frac{1}{N} \sum_{k=1}^{N} \left| \frac{\psi_k^i - \psi_k^{i-1}}{\psi_k^{i-1}} \right|$$

be less than 10^{-5}, where N is the number of cells, i is the numerical step, and ψ is either the macroscopic velocity v or the density ρ. With such a choice we adopted a grid of 100×100 cells of constant steps $\Delta\xi$ and $\Delta\eta$ and a maximum number of representative particles equal to 1,000,000.

Note that a uniform grid in the bipolar domain corresponds to a non-constant distribution of the steps and of the area of the cells in the physical space between the two cylinders. In particular the elemental area in the (ξ, η) domain is given by

$$A(\xi, \eta) = \iint \frac{1}{(\cosh \xi + \cos \eta)^2} \, \mathrm{d}\xi \, \mathrm{d}\eta.$$

In such a way the cells of minimum size are located close to the inner cylinder, where separation may occur. The choice of fine grid while increasing the space resolution of the field must be, at the same time, balanced by a sufficient number of particles observed in each elemental area to provide meaningful statistics. Therefore the steps of the coordinates and the distribution of the elemental areas are equally important in the DSMC. This was fully described in [1]. We just add a few notes here. Let $\eta = \pi$ and $\bar{\xi} = (\xi - \xi_i)/(\xi_e - \xi_i)$. For $\Delta\bar{\xi} = 0.01$ and $\Delta\eta = 2\pi \times 10^{-2}$, Table 1 shows, in a significant case, $\bar{r}_k = (r(\xi_k) - r(\xi_i))/(r(\xi_e) - r(\xi_i))$ varies with $\bar{\xi}_k$. Also shown are the increasing variations with $\bar{\xi}_k$ of the step in the physical plane $\Delta r_k = r(\xi_k) - r(\xi_{k-1})$ and of the ratio of the cell area ΔA_k at $\bar{\xi}_k$ to its maximum value $\Delta A_{\max}$ at $\bar{\xi}_k = 1$.

Table 1
Mesh distribution for $\eta = \pi$, $\epsilon = 0.60$, $\overline{R} = 0.5$, $\Delta\eta = 2\pi \times 10^{-2}$

$\bar{\xi}_k$	$\bar{r}_k$	$\Delta\bar{\xi}_k$	$\Delta r_k \times 10^2$	$\Delta A_k/\Delta A_{\max}$
0.01	0.0056	0.01	0.432	0.2076
0.05	0.0358	0.01	0.449	0.2223
0.10	0.0658	0.01	0.472	0.2382
0.50	0.3794	0.01	0.720	0.4293
0.75	0.6455	0.01	0.959	0.6461
1.00	1.0000	0.01	1.291	1.0000

3. Results and conclusion

An analysis of the Stokes flow predicts that a pair of separation points exists on the stationary cylinder provided that the eccentricity exceeds a critical value which depends on the ratio $\overline{R}$. These points change their positions as a consequence of the inertial effects. In a rather old article, Ballal and Rivlin [7] carried out a detailed analysis of the flow by means of the Navier–Stokes equation in the case of an incompressible fluid. By a linearized approximation of the inertial effects they established a number of conditions under which separation points and eddies exist.

Figs. 2(a), 2(b) present some details of the evolution of the velocity vector profiles and some streamlines as affected by Kn_0. This solution is for $\overline{R} = 0.5$, $\epsilon = 0.45$, and $Ma_e = 0.5$. As a reference, the Stokes flow solution for the tangential velocity profile at $\eta = \pi$ is also given in Fig. 2(c) together with the solutions for $Kn_0 = 0.1$ and 1.

In Figs. 2(a), 2(b) the Cartesian dimensionless co-ordinates x, y, are centered in O_i and their values are recovered from ξ, η through the proper transformation formulae. This Cartesian set greatly simplifies the determination of the vortex center. The figures show qualitatively the enlarged region where separation occurs for $Kn_0 = 0.1$, whereas for $Kn_0 = 1$ separation just vanished. Let α_a be the displacement of the vortex center, r_a its distance from the inner wall and $\Delta\eta_s$ the distance from the separation and reattachment points. From numerical data of this kind the extent of the separated region $\Delta\eta_s$ on the inner wall and the polar coordinates (r_a, α_a) of its axis were evaluated and are reported in Tables 2 and 3. The same quantities were also calculated from the analytic expressions for the Stokes flow, as we will see. When Fig. 2(c) is considered, the v-profiles at $\eta = \pi$ correspond to the section of maximum gap D between the walls. The reference horizontal abscissa is there $\bar{r} = (r - R_i)/D$. Figs. 2(a)–(c) help to clarify the noticeable changes of flow geometry as a function of Kn_0 variations, and these variations will significantly influence the τ and $\dot{q}_\xi$ distributions.

Note that the Stokes' solution was obtained by imposing the no-slip at the wall condition. The direct simulation provides – as a result – the flow velocity at the wall. The slip – of course – increases with the local value of the Knudsen number. Fig. 2(c) clearly shows that the velocity at the inner wall is different from zero and increases with rarefaction. In particular its value is small but negative when separation is present (case (a)). At the outer wall, where the density value is maximum due to the centrifugal force, the local Kn is almost the same in both cases (a) and (b) and the slip velocity is almost the same.

Figs. 3–5 show the shear stress distributions at the walls vs η/π, for various ϵ, as functions of Kn_0. Fig. 3 presents the Stokes solutions for values of the eccentricity greater than the critical value $\epsilon_{cr} = 0.27$ from which the onset of recirculation begins, according to the analytic solution. In the separated region the τ_e profile first flattens with increasing ϵ and then changes the sign of its curvature. In the particular case of Stokes flow the reference dimensional value of the shear stress was assumed equal to the one adopted for the case in Fig. 4.

In Figs. 4 and 5 we note that the effect of the inertial term is to move the region of higher τ downstream, as is also the case for a continuum gas. As shown in Figs. 2(a) and 2(b), for a $Ma_e = 0.5$ the eddy which is present for $Kn_0 = 0.1$ and $\epsilon = 0.45$ disappears for $Kn_0 = 1$. For the cases in Fig. 4, where $Ma_e = 0.5$, $Kn_0 = 0.1$, we calculated $\epsilon_{cr} > 0.30$, and for those in Fig. 5, where $Ma_e = 0.5$ and $Kn_0 = 1.0$, we obtained $\epsilon_{cr} > 0.45$.

The influence of the separated region clearly appears on the τ_i distribution and on the derivative $d\tau_i/d\eta$. Note that the onset condition for separation is the vanishing of the normal derivative of the velocity at the wall at rest. However the value $\tau_e = 0$ does not correspond to the onset of separation at the moving external surface where this condition only means that the flow is locally changing its profile either from greater to lower speeds than the speed of the wall or vice-versa (see, e.g., Fig. 5). An example of the heat flux distributions at the walls is reported in Fig. 6 for $Kn_0 = 0.1$ and three values of the eccentricity.

As for τ, the influence of the separated region on $\dot{q}_\xi$ and $d\dot{q}_\xi/d\eta$ at the cylinder's surfaces is evident. We note the analogy to the τ distributions and the increase of the local heat transfer through the isothermal walls as the eccentricity increases. The energy transferred to the fluid by the wall rotation is dissipated by the fluid, and is equal to the net heat transfer at the walls. We also note that there are tracts of the two surfaces through which heat is supplied to the fluid and others where the heat flux is leaving while the walls are kept at constant temperature.

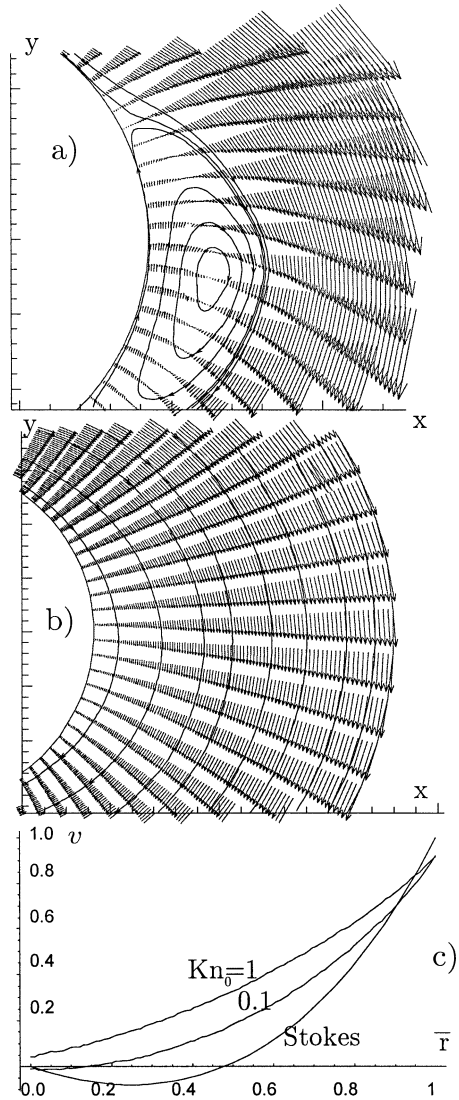

Fig. 2. Flow field characteristics for $Ma_e = 0.5$, $\epsilon = 0.45$, $\overline{R} = 0.5$. Velocity vector and streamlines (a) $Kn_0 = 0.1$, (b) $Kn_0 = 1$. Velocity profiles at $\eta = \pi$ for different rarefaction levels.

Table 2
Rarefaction effects on the eddy extension and location for $Ma_e = 0.5$, $\epsilon = 0.60$, $\overline{R} = 0.5$

Kn_0	r_a	α_a (rad)	$\Delta\eta_s$ (rad)
0.01	1.867	−0.135	2.450
0.1	1.618	−0.141	1.571
1.0	1.273	−0.200	1.006
10	1.236	−0.220	0.754

Mapping the values of the Mach number and of the dimensionless temperature leads to the results in Figs. 7–11. The kinetic and thermal fields for $Ma_e = 0.5$, $Kn_0 = 0.1$ are shown, as a functions of ϵ, in Figs. 7 and 8, respectively. Fig. 9 reports the temperature map as function of Kn_0, for $Ma_e = 0.5$ and for $\epsilon = 0.6$, and the final Figs. 10 and 11 show the analogous maps of Ma and T as Ma_e takes three values for $\epsilon = 0.45$ and $Kn_0 = 0.1$.

Table 3
Effects of the external wall velocity on the extension and location of the eddy for $Kn_0 = 0.1$, $\epsilon = 0.45$, $\overline{R} = 0.5$

Ma_e	r_a	α_a (rad)	$\Delta\eta_s$ (rad)
0.5	1.386	−0.369	1.068
1	1.216	−0.398	0.807
2	1.140	−0.451	0.754

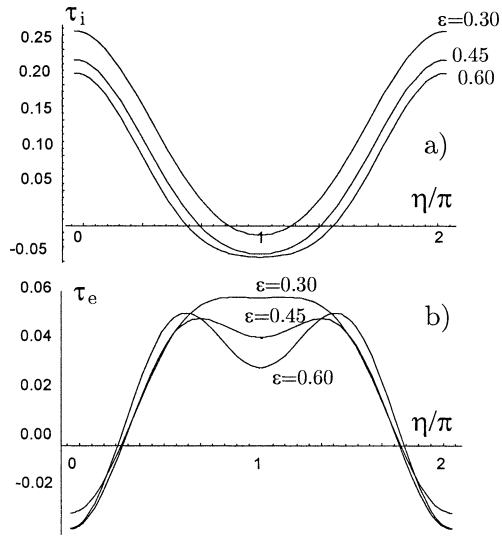

Fig. 3. Shear stress distribution in Stokes flow for various ϵ. (a) inner wall, (b) outer wall.

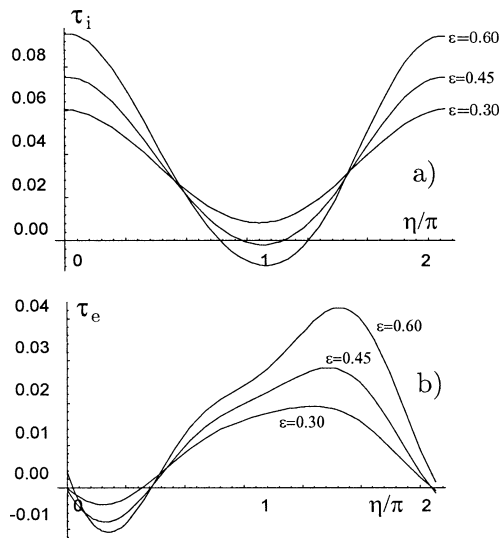

Fig. 4. DSMC results. Shear stress distribution for various ϵ, $Kn_0 = 0.1$, $Ma_e = 0.5$, $\overline{R} = 0.5$ (a) inner wall, (b) outer wall.

At a first sight, the maps confirm some observations already made concerning the inertial and rarefaction effects. In particular an increasing ϵ moves the separated vortex downstream with respect to the Stokes solution. In addition an increasing Ma_e tends to reduce the size of the vortex while moving its axis further downstream, all other parameters being kept equal. We recall that in the incompressible Navier–Stokes case it was shown [7] that at increasing (although very small) Reynolds numbers Re_0 the vortex moves upstream provided that the eccentricity is less than a limit value ϵ_{lim} which depends on $\overline{R}$ and Re_0. That analysis

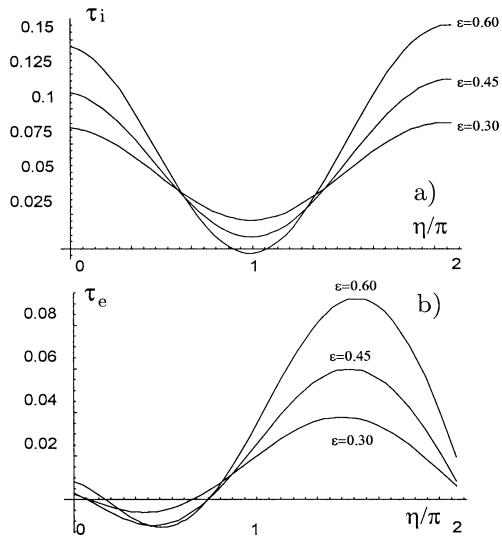

Fig. 5. DSMC results. Shear stress distribution for various ϵ. $Kn_0 = 1$, $Ma_e = 0.5$, $\overline{R} = 0.5$. (a) inner wall, (b) outer wall.

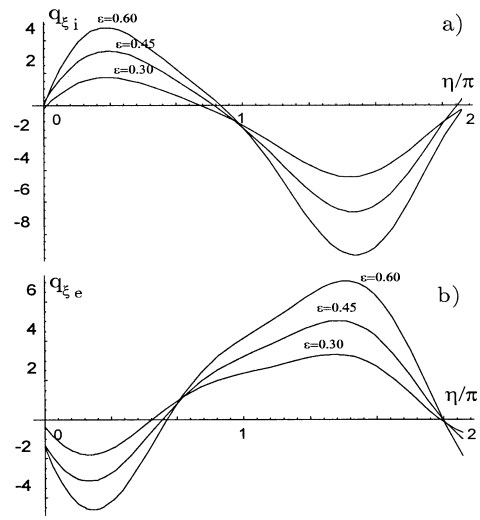

Fig. 6. DSMC results. Heat flux distribution for various ϵ. $Kn_0 = 0.1$, $Ma_e = 0.5$, $\overline{R} = 0.5$. DSMC results. (a) inner wall, (b) outer wall.

also showed that, for $\epsilon > \epsilon_{\text{lim}}$, the vortex moves instead downstream with respect to the Stokes flow solution. In a compressible gas Re_0 is proportional to Ma_e/Kn_0. In all the Ma_e and Kn_0 cases which we consider here are, the corresponding values of Re_0 are such that this inversion cannot be detected.

At this point the main effects of the dimensionless numbers on changing the field characteristics can be realized. Fig. 7 shows how the vortex, which is just appearing for $\epsilon_{cr} = 0.30$ and extends itself with increasing ϵ, is lowering the *Ma* values in the slower region while is increasing the *Ma* values in the faster region. At the same time the shear stress distribution and, consequently, the region of maximum dissipation and its importance change. In Fig. 8 we note that the difference between the maximum and the minimum values of T increases with ϵ. We also observe here from Fig. 9 that an increase of rarefaction, for Kn_0 ranging between 0.01 and 100, makes the mean value of T to increase in the domain. What is interesting is the displacement of the colder region toward the wider gap with a decreasing ϵ. We also report from our calculations that, although the values of T do change with Kn_0, for $Kn_0 \geqslant 1$ at constant ϵ, the temperature maps all look alike as far as the distribution of the colder and hotter regions is concerned. This fact can be realized when one recalls that, as the rarefaction increases, the molecular collisions against the walls prevail with respect to those between the molecules. As a consequence conduction through the fluid becomes weaker and weaker as Kn_0 increases.

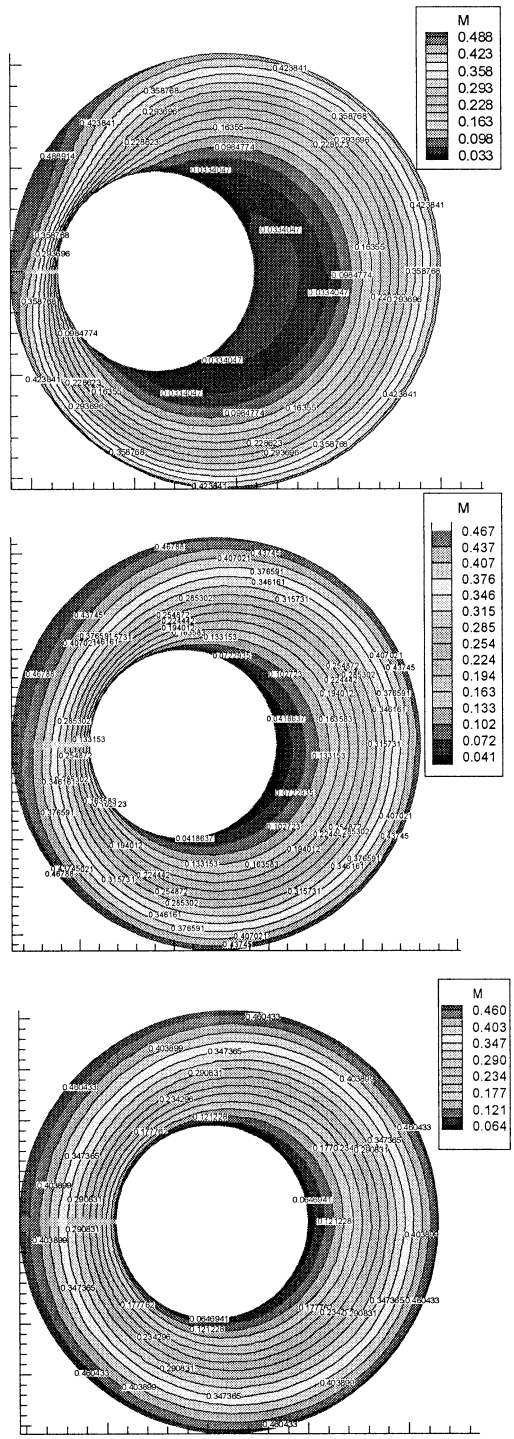

Fig. 7. Mach number distribution for $Ma_e = 0.5$, $Kn_0 = 0.1$, $\overline{R} = 0.5$. Top: $\epsilon = 0.60$; middle: $\epsilon = 0.30$; bottom: $\epsilon = 0.15$.

Figs. 10 and 11 show the effects of an increasing Ma_e on the kinetic and thermal fields. The trends already shown in Figs. 7 and 8 are confirmed by the case on top of Figs. 10, 11 which is relative to $\epsilon = 0.45$. Our calculation show that an increasing Ma_e in the range 0.5–2 increases a sustainable ϵ before separation occurs. Furthermore both the colder and the warmer regions

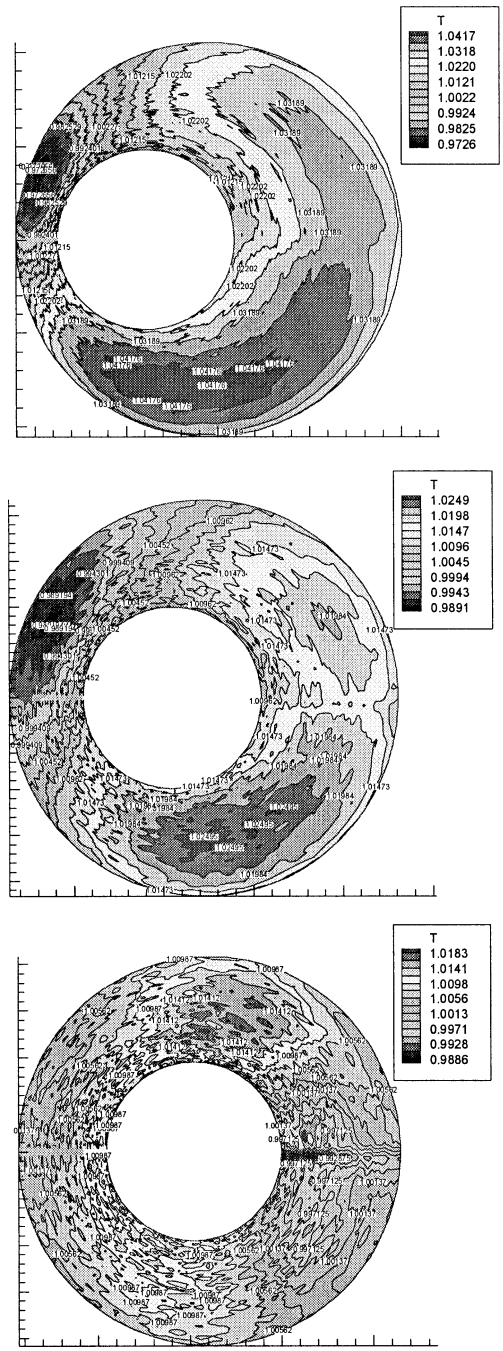

Fig. 8. Temperature distribution for $Ma_e = 0.5$, $Kn_0 = 0.1$, $\overline{R} = 0.5$. Top: $\epsilon = 0.60$; middle: $\epsilon = 0.30$; bottom: $\epsilon = 0.15$.

move in the direction of rotation and the same is true for the slower and faster regions at constant Kn_0 and Ma_e. Due to the increased shear stresses at greater Ma_e, T_{max} also increases whereas T_{min} decreases.

While the presence of regions at temperatures greater than the wall temperature is easily understood, less intuitive is the presence of regions cooler than the boundaries.

In this respect let us observe that zones at greater local *Ma* correspond to lower values of the temperature or, in other words, to greater kinetic energies of the ordered macroscopic motion correspond lesser values of the disordered microscopic energy. The kinetic energy dissipated in the slower regions at higher pressure partially leaves through the walls. As the fluid

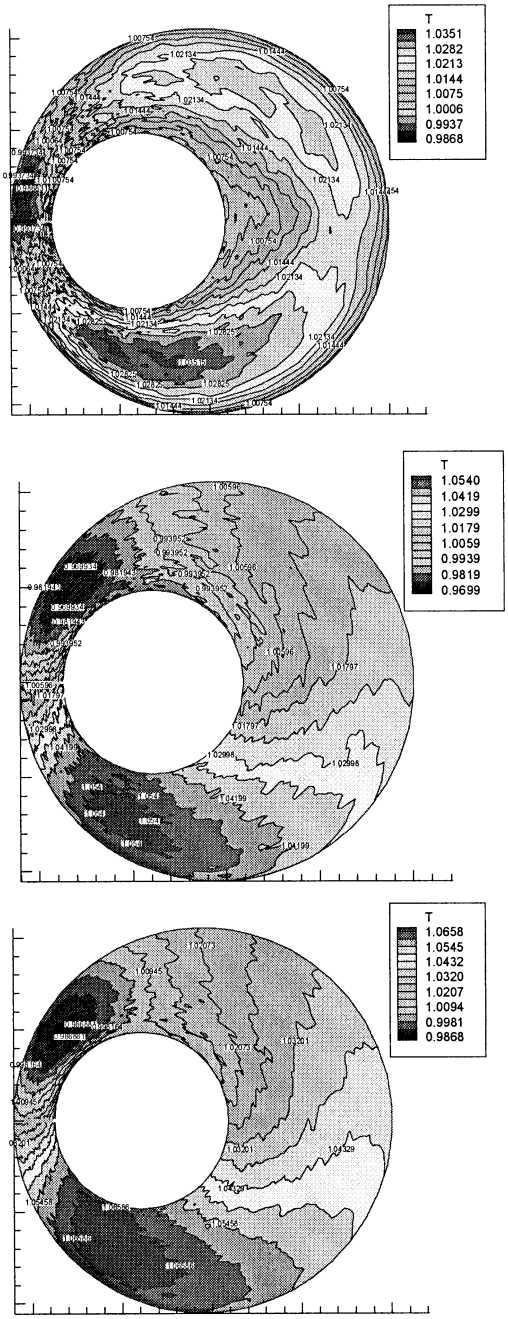

Fig. 9. Temperature distribution for $Ma_e = 0.5$, $\epsilon = 0.60$, $\overline{R} = 0.5$. Top: $Kn_0 = 0.01$; middle: $Kn_0 = 1$; bottom: $Kn_0 = 100$.

flow proceeds through the regions where – to keep its mass continuity – its speed must increase, its pressure decreases and so does the temperature. The preceding loss of internal energy is not balanced by the heat transfer at the walls and by the heat dissipation. We recall that an increase of rarefaction makes the heat transfer coefficient at the walls to decrease at constant Ma_e due to the corresponding temperature jump at the interface.

Some concluding results are provided in Tables 2 and 3 which give the characteristics of the vortex evolution as functions of Kn_0 and Ma_e (recall that $Re_0 \propto Ma_e/Kn_0$). Then Table 2 shows that $\Delta\eta_s$ is definitely decreased by the gas rarefaction while the vortex center gets closer to the inner wall and moves downstream. Table 3 provides an indication of the effects of the external wall velocity on the separated region. Increasing Ma_e reduces the vortex extent while moving the center downstream

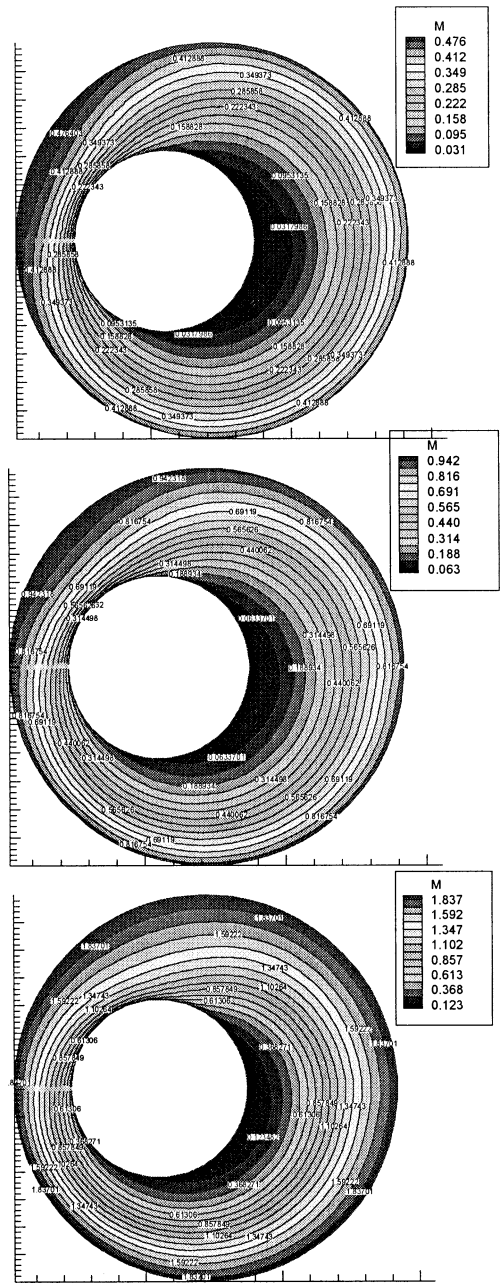

Fig. 10. Mach number distribution for $\epsilon = 0.45$, $Kn_0 = 0.1$, $\overline{R} = 0.5$. Top: $Ma = 0.5$; middle: $Ma = 1.0$; bottom: $Ma = 2.0$.

and closer to the wall. By comparing the results in Tables 2 and 3 relative to the case $Kn_0 = 0.1$ and $Ma_e = 0.5$ we note that at increasing ϵ corresponds a lesser downstream, α_a whereas r_a and $\Delta\eta_s$ both increase. As a comparison we cite that the Stokes flow solution for $\epsilon = 0.45$ is $r_a = 1.707$, $\Delta\eta_s = 1.390$, and for $\epsilon = 0.60$ is $r_a = 1.810$, $\Delta\eta_s = 1.745$, α_a being zero in both cases.

As a final conclusion we see that the Monte Carlo Direct Simulation is effective in providing insight into some relevant physical aspects of a complex flow situation. The opposite influences of eccentricity and gas rarefaction on the vortex characteristics and their dependence on the wall velocity were satisfactorily described. In addition, the noticeable influence of the Knudsen number in locating flow regions which are cooler than the walls was investigated.

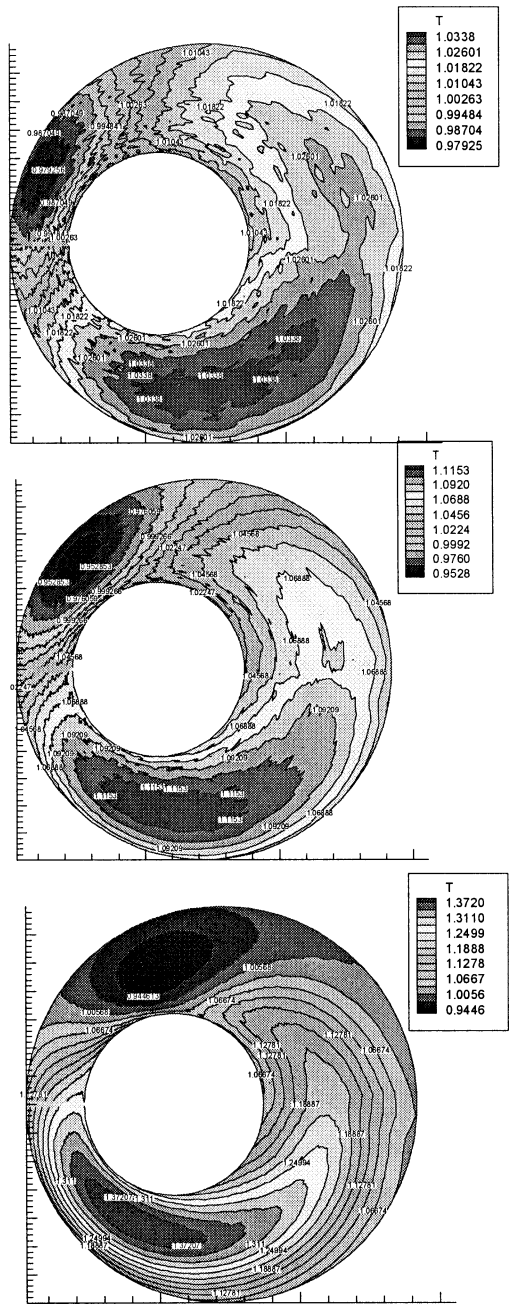

Fig. 11. Temperature distribution for $\epsilon = 0.45$, $Kn_0 = 0.1$, $\overline{R} = 0.5$. Top: $Ma = 0.5$; middle: $Ma = 1.0$; bottom: $Ma = 2.0$.

Acknowledgement

This work was partially supported by MURST and ASI 99-195.

References

[1] L.M. de Socio, L. Marino, Numerical experiments on the gas flow between eccentric rotating cylinders, Int. J. Numer. Methods Fluids 34 (3) (2000) 229–240.

[2] A.Z. Szeri, Fluid Film Lubrication. Theory and Design, Cambridge University Press, Cambridge, UK, 1998.
[3] L.M. de Socio, N. Ianiro, L. Marino, Effect of the centrifugal forces on a gas between rotating cylinders, AIAA J. Thermophys. Heat Transfer 14 (2) (2000) 269–275.
[4] F.M. Sharipov, G.M. Kremer, Nonlinear couette flow between two rotating cylinders, Transport Theory Statist. Phys. 25 (1996) 217–229.
[5] C. Cercignani, F. Sernagiotto, Cylindrical couette flow of a rarefied gas, Phys. Fluids 10 (1967) 1200–1204.
[6] G.J. Farris, Flow in a journal bearing, M.S. Thesis, North-Western University, Evanston, IL, 1962. Reported in: R. Enrhlich, C.J. Slattery, Evaluation of power-model lubricants in an infinite journal bearing, I & E C Fundamentals 7 (1968) 239–240.
[7] B.Y. Ballal, R.S. Rivlin, Flow of a Newtonian fluid between eccentric rotating cylinders: inertial effects, Arch. Rational Mech. Anal. 62 (1977) 237–294.
[8] W.W. Wood, The asymptotic expansions at large Reynolds numbers for steady motion between non-coaxial rotating cylinders, J. Fluid Mech. 8 (1957) 159–175.
[9] J.H.C. Araujo, V. Ruas, A.S. Vargas, Finite element solution of flow between eccentric cylinders with viscous dissipation, Int. J. Numer. Methods Fluids 11 (1990) 849–865.
[10] P.M. Gresho, R.L. Lee, R.L. Sani, M.K. Maslanik, B.E. Eaton, The consistent Galerkin FEM for computing derived boundary quantities in thermal and/or fluids problems, Int. J. Numer. Methods Fluids 7 (1987) 371–394.
[11] L.M. de Socio, N. Ianiro, L. Marino, Rarefied gas flow between eccentric cylinders, Int. J. Appl. Sci. Comput. 7 (1) (2000) 49–57.
[12] R.G. Bird, Molecular Gas Dynamics and the Direct Simulation of Gas Flows, Clarendon Press, Oxford, UK, 1994.
[13] F.J. Alexander, A.L. Garcia, B.J. Alder, Cell size dependence of transport coefficients in stochastic particle algorithms, Phys. Fluids 10 (1998) 1540–1542.
[14] A.L. Garcia, W. Wagner, Time step truncation error in direct simulation Monte Carlo, Phys. Fluids 12 (2000) 2621–2633.
[15] N. Hadjiconstantinou, Analysis of discretization in the direct simulation Monte Carlo, Phys. Fluids 12 (2000) 2634–2638.